In-situ synthesis of aluminum/nano-quasicrystalline Al-Fe-Cr composite by using selective laser melting

N. Kang, M. El Mansori, X. Lin, F. Guittonneau, H.L. Liao, W.D. Huang, C. Coddet

▶ **To cite this version:**

N. Kang, M. El Mansori, X. Lin, F. Guittonneau, H.L. Liao, et al.. In-situ synthesis of aluminum/nano-quasicrystalline Al-Fe-Cr composite by using selective laser melting. Composites Part B: Engineering, 2018, 155, pp.382-390. 10.1016/j.compositesb.2018.08.108 . hal-02417272

HAL Id: hal-02417272
https://hal.science/hal-02417272

Submitted on 18 Dec 2019

HAL is a multi-disciplinary open access archive for the deposit and dissemination of scientific research documents, whether they are published or not. The documents may come from teaching and research institutions in France or abroad, or from public or private research centers.

L'archive ouverte pluridisciplinaire **HAL**, est destinée au dépôt et à la diffusion de documents scientifiques de niveau recherche, publiés ou non, émanant des établissements d'enseignement et de recherche français ou étrangers, des laboratoires publics ou privés.

In-situ synthesis of aluminum/nano-quasicrystalline Al-Fe-Cr composite by using selective laser melting

N. Kang[a,b,*], M. El Mansori[c,e], X. Lin[a,b], F. Guittonneau[c], H.L. Liao[d], W.D. Huang[a,b], C. Coddet[d]

[a] State Key Laboratory of Solidification Processing, Northwestern Polytechnical University, Xi'an, Shaanxi, 710072, PR China
[b] Key Laboratory of Metal High Performance Additive Manufacturing and Innovative Design, MIIT China, Northwestern Polytechnical University, Xi'an, Shaanxi, 710072, PR China
[c] MSMP Laboratory, EA-7350, Arts et Metiers ParisTech, Aix en Provence, 13617, France
[d] University Bourgogne Franche-Comte, IRTES EA7274, F-90100, Belfort, 90400, France
[e] Texas A&M Engineering Experiment Station, College Station, TX, 77843, USA

Keywords:
Selective laser melting
Quasicrystal
Microstructure
Annealing
Tensile

A B S T R A C T

In this research, Al-Fe-Cr quasicrystal (QC) reinforced Al-based metal matrix composites were *in-situ* manufactured by using selective laser melting (SLM) from the powder mixture. The parametrical optimization based on our previous work was performed with focus on laser scanning speed. From the optimized parameters, an almost dense (99.7%) free-crack sample was fabricated with an ultra-fine microstructure. A phase transition from decagonal QC $Al_{65}Cu_{25}Fe_{10}Cr_5$ to icosahedral QC $Al_{91}Fe_4Cr_5$ could be observed as laser scanning speed decreases. Differential scanning calorimetry curves show that the QC phase is quiet stable until 500 °C. And then, the effects of annealing temperature on the microstructural and mechanical properties were determined. The results indicate that the recrystallization and growth behavior of α-Al grains could be prevented by QC particle during annealing. Furthermore, the growth of QC particle, which tends to form a porous structure, leads an improvement of Young modulus and decline of ductility.

1. Introduction

Due to the high strength, low friction coefficient and high corrosion/wear resistances, quasicrystal is extremely investigated and developed in the past decades [1,2]. In general, the quasicrystalline structures are presented as two categories: (I) icosahedral (i-hereafter) and (II) decagonal (d-) point group symmetries [3]. Up to now, quasicrystalline phase has been observed in over 100 different alloy systems with the different industrial applications [4,5]. However, the quasicrystal shows intrinsic brittleness due to its complex crystalline structure, so it is very difficult to be prepared in complex forms by using conventional manufacturing process [6], which limits their potential applications. The possibilities of circumvent their intrinsic brittleness with keeping their useful properties are to use them as coating material or reinforcement in composite material by profit from the high ductility of substrate/matrix material. For example, the thermal spraying technology is considered as an effective way to produce the pure QC coatings [6,7] and their composites [8,9].

Recently, additive manufacturing (AM) presents great advantage in producing the sophisticated component with minimal material waste, which is difficult or impossible to be manufactured through traditional subtractive methods [10,11]. Selective laser melting (SLM) is a promising processing method to fabricate near net-shaped 3D components with customized geometries and properties [12]. In this process, the component is firstly designed in 3D model by using a computer-aided design (CAD) software, after that, this mode is sliced into 2D layers with a very low thickness (from 20 μm to 100 μm). Then, a computer controlled high-power-focused laser selectively scans the powder bed, the scanned powder is fully melted accompany with a rapid solidification. As it finished, the build platform descends by one layer thickness and then a new layer of powder is deposited on top. Such a layer by layer process continuous until the objective component completely formed [13]. Due to the small diameter of laser beam and low powder thickness, the interaction volume is well restricted. Additionally, the interaction time (mille second) between the laser beam and material during SLM is very short. Therefore, it creates ultra-high cooling rate (about 10^3–10^7 K/s) [14,15].

The feedstock materials for SLM process are usually pre-alloyed commercial powders, such as AlSi10 Mg [16], 316steel [17], Ti6Al4V [18] etc., which provide great advantages in homogeneity and chemical

* Corresponding author. State Key Laboratory of Solidification Processing, Northwestern Polytechnical University, Xi'an, Shaanxi, 710072, PR China.
E-mail address: nan.kang@nwpu.edu.cn (N. Kang).

stability. However, the limitation in composition flexibility and high cost should also be considered [19]. Powder mixture provides one possible method to innovate the new materials with high composition flexibility, low energy consummation and processing materials with high melting temperature by SLM [20,21]. Kang et al. [22] investigated the microstructural and mechanical properties of SLM processed Al-12Si from pre-alloyed and mixed powder. They indicated that the *in-situ* method (powder mixture) presents an acceptable difference with pre-alloyed method.

Recently, additive manufacturing is considered as an important process to produce the complex component with high strength and high tenacity Al-based alloys [23]. Moreover, the *in-situ* prepared Al-matrix composite gives consideration to both composite structural properties and interfacial problem. Thus, in this study, Al-based QC reinforced system was selected, due to its low density, high forming ability and potential *in-situ* reaction between matrix and reinforcement. The pore and crack free composite sample was successfully manufactured with optimized parameters. The microstructural and tensile properties of as-fabricated and heat-treated samples were analyzed with a special emphasis on the phase transition and interface properties.

2. Experimental details

$Al_{65}Cu_{20}Fe_{10}Cr_5$ QC (d (50) = 45 μm) and pure Al (d (50) = 20 μm) powders produced in laboratory via gas atomization under argon atmosphere (Nanoval process)) were used (see in Fig. 1 (a)). The QC and Al powders were blended with a weight proportion of QC: Al = 30: 70 in a tumbling mixer for 120 min ((TURBULA, Switzerland)) and dried at 80 °C for 4 h before use. The surface morphologies of powder mixture were shown in Fig. 1 (a). It can be observed that the QC particles illustrate a relative uniform distribution in the powder mixture, because the absolute densities and particle sizes of these two powders are comparable. Moreover, both the two powders particles possess a spherical shape and are characterized by a low amount of satellites, whereby smaller particles (fewer than 10 μm) are adhered to the large particle surface.

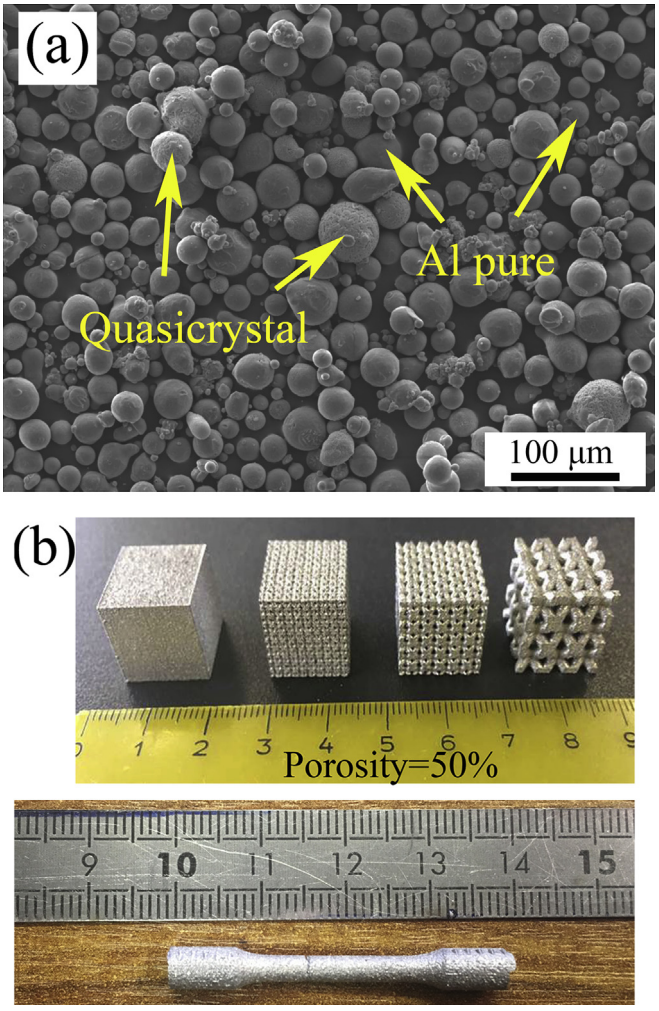

Fig. 1. (a) Morphology of feedstock powder mixture of Al pure and QC, (b) as-fabricated dense and porosity of 50% cubic parts and tensile sample.

A commercial SLM machine MCP-realizer SLM 250 equipped with YLR-100-SM single-mode CW ytterbium fiber laser (MCP-HEK Tooling GmbH, Germany) was employed. Small cube ($8 \times 8 \times 8\ mm^3$) and cylindrical tensile samples (see in Fig. 1 (b)) were fabricated using zigzag scanning mode under argon environment (oxygen content < 0.2%). Some lattice cubic samples with porosity of 50% (different pore sizes) were also prepared, which are illustrated Fig. 1 (b). Laser power, layer thickness and hatch distance are set as 300 W, 50 μm and 120 μm respectively. A pure Al substrate was sandblasted before process, and heated to 125 °C during the process. The heat treatments were performed in an electric furnace (SCFEB, France) under air condition.

X-ray Diffraction (XRD) was performed on a Siemens apparatus with a Cobalt anticathode (λ = 1.78897 Å) operated at 35 kV and 40 mA. The microstructure was observed by scanning electron microscopy (SEM) (JEOL JSM-5900LV and JSM-7001F, Japan) equipped with X-ray energy dispersive spectroscopy (EDS) and an Oxford Nordlys-HKL EBSD detector. The interfacial microstructures were characterized by Transmission Electron Microscopy (TEM, JEM2100F, JEOL). Before characterization of TEM, the test samples were prepared by Focused Ion Beam (FIB, 450S, FEI) milling. This technique was chosen due to the advantage of high grain contrast obtained when imaging with ions and stress free preparation. The thermal properties of SLM processed sample were determined by Differential Scanning Calorimetry (DSC) test under argon environment from 30 °C to 800 °C with a heating rate of 20 °C/min (NETZSCH, Germany). Microhardness was measured on polished samples (Ra = 0.02 μm) with a Vickers indenter at load of 200 g and a dwell time of 25 s. A Lloyd Instrument testing machine (LR50K, USA) was employed to perform the tensile test with a constant traverse speed of 1 mm/min. Each tensile test was preformed 3 times to obtain an average value. Tensile fracture surfaces of the test specimens were observed by using SEM.

3. Results and discussions

3.1. As-fabricated QC composite

The area fraction of porosity, which is measured by image analysis from 30 pictures at 3 different altitudes, is shown in Fig. 2. It can be seen that the relative density of SLM processed composite sample can reach to 99.7% with laser scanning speed of 2 m/s. Moreover, the graph also shows that there has been a steady increase of porosity from 0.3% to 32%, when laser scanning speed increases from 2 m/s to 8 m/s. It is worthy to note that as laser scanning speed is superior to 3 m/s, the porosity rises rapidly from 5% to 15%. This extensive increment of porosity causes significant influence on microstructural and mechanical properties. Therefore, 3 m/s can be defined as the critical laser scanning speed for this composite system [13].

The XRD patterns of SLM processed samples (over and local views) are presented in function of laser scanning speed in Fig. 3. Overall speaking, the SLM processed sample mainly consists by matrix α-Al and QC phase. From the overview patterns in Fig. 3 (a), the matrix α-Al phase presents a high intensity with the peak of θ-phases Al_2Cu, which was also observed in QC powder [6]. The formation of Al_2Cu phase could be attributed to: (1) Al_2Cu cell is more stable than AlCu, given to the small size of Al_2Cu; (2) the high content of Al is beneficial to from Al-rich phase. In general, laser scanning speed shows no clearly

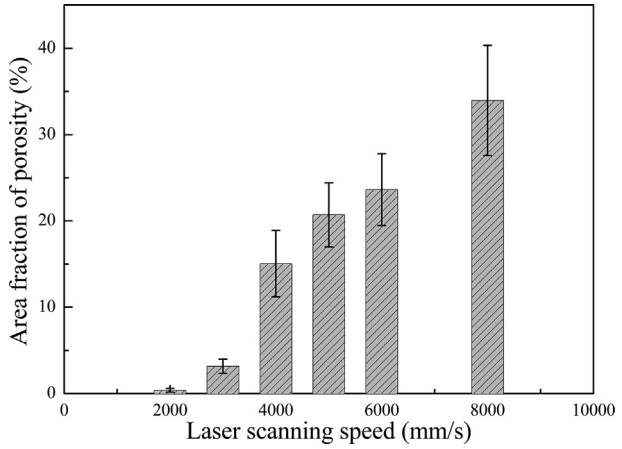

Fig. 2. Porosity analyses of SLM processed samples with several laser scanning speeds from 2 m/s to 8 m/s.

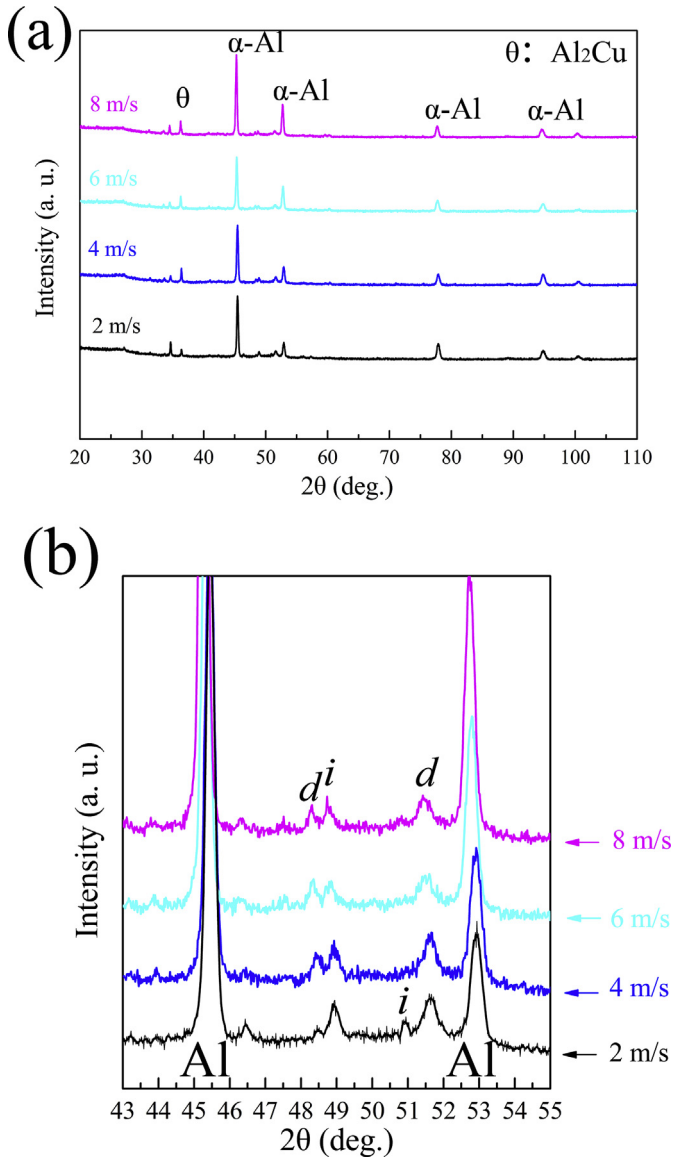

Fig. 3. (a) overview and (b) local view XRD patterns of SLM processed sample with several laser scanning speeds.

influence on α-Al and θ-phases. A detailed analysis ranged 43°–55° is shown in Fig. 3 (b). It indicates that a phase transition from decagonal (*d*-) QC $Al_{65}Cu_{25}Fe_{10}Cr_5$ to icosahedral (*i*-) QC $Al_{91}Fe_4Cr_5$, as laser scanning speed decreases from 2 m/s to 8 m/s. According to the report of Dubois et al. [24], a reversible crystal-quasicrystal transition, which is affected by the chemical composition, was observed in Al-Cu-Fe QC. In this work, as laser scanning speed declines, both the QC and Al could be fully melted and further mixed. Therefore, the increment of Al content in metallic liquid leads to phase transition from *d*-$Al_{65}Cu_{25}Fe_{10}Cr_5$ to *i*- $Al_{91}Fe_4Cr_5$ during the solidification.

During SLM process, the high temperature gradient of molten pool induces circulation of the molten material driven by surface tension gradient and non-equilibrium of solid-liquid interface. This flow of metal liquid, which is also called Marangoni effect, can include the incomplete melted particle. In order to investigate the interactive behavior between reinforcement and matrix during SLM process, the interfacial microstructure between partial melted QC and α-Al of as-fabricated sample is shown in Fig. 4. As shown in Fig. 4(a and b), the microstructure of FIB prepared sample can be divided into three different types: (I) the unmelted QC particle with a dense structure; (II) the interfacial region consisted by bar-liked QC and Al; (III) the composite region consisted by small spherical QC phase and Al matrix. TEM elemental analysis (see in Fig. 4(c–f)) results show that the Kirkendall effect could be observed at the interface region of SLM processed composite. In detail, Fe and Cr elements are few diffused; in contrast, Cu shows high diffusion coefficient with Al matrix. Similar result is reported by Bergmann et al. in case of Al-Cu welding [25]. Thus, this diffusion behavior causes the composition modification and then phase transition from Al-Cu rich QC to Al rich QC.

According to the relative position of QC to laser beam, the melting, reacting and solidification behavior (MRS) behavior can be illustrated into two models, which are shown in Fig. 5. For the QC particle, which is scanned directly by laser (particle 1 and 2 in Fig. 5 (a)), it is fully melted and mixed with Al liquid. Then, the QC phase is separated out from the metal liquid during the solidification behavior. Because the QC phase possesses higher melting temperature than that of α-Al, thus it acts as nucleation center (see in Fig. 9 (a)). If the QC particle is out of laser beam, such as particle 3 and particle 4 in Fig. 5 (a), this MRS behavior is illustrated in Fig. 5 (b). Firstly, the QC particle is immerged into the molten pool and then stripped into small fragments from powder surface by the Marangoni effect. After that, the QC fragment forms the novel QC phases by in-situ diffusion reaction with Al matrix.

Fig. 6 shows the DSC curves from room temperature to 800 °C of SLM processed samples with different laser scanning speeds. For all the samples, a clearly decalescence behavior appears near 600 °C, which corresponds to molten of matrix material α-Al [26]. Furthermore, the sample processed at higher laser scanning speed illustrates smaller decalescence peak area than that of low scanning speed sample. In details, when the laser scanning speed rises from 2 m/s to 8 m/s, the absorbed heat decreases from 221.21 J/g to 184.99 J/g (see Fig. 6(a–d)), which indicates the decrement of α-Al phase. It can be attributed to that the QC particle only be partial melted in case of high laser scanning speed. On the other hand, the small exothermic peaks (indicated by red narrow in Fig. 6(a–d)) appear at the temperature in range from 500 °C to 520 °C. Galano et al. [4] reported the similar result in the case of melt spinning Al-Cu-Fe-Cr, which represents the growth of i-QC phase and the phase transition. Thus, from to the results of DSC analysis, the heat treatment temperatures are chosen at 450 °C, 480 °C (before growth of QC), 510 (during growth of QC) and 540, 570 °C (after growth of QC, before melting of Al) for 30 min with air cooling condition.

3.2. Heat treated QC composite

The OM images of as-polished SLM processed samples in condition of as-fabricated and heat treated are shown in Fig. 7. The similar

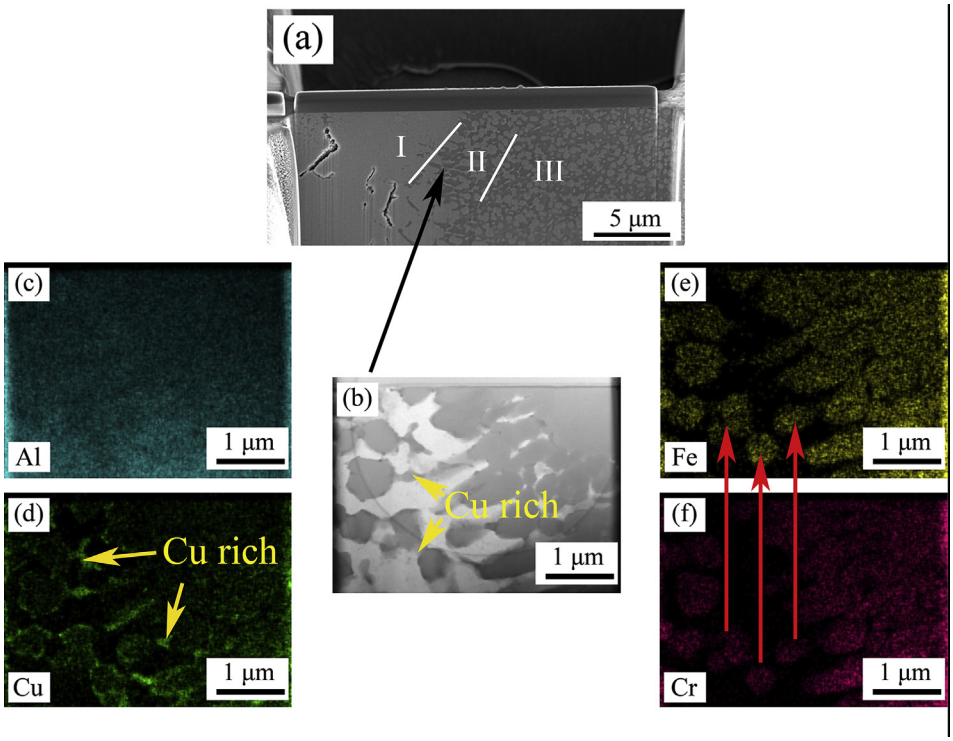

Fig. 4. Interfacial microstructure between partial melted QC reinforcement and α-Al of as-fabricated sample: (a) FIB prepared sample, (b) interfacial region and element distribution (c) Al, (d) Cu, (e) Fe and (f) Cr.

porosity content can be observed on all the samples, which indicates that the effect heat treatment on the porosity can be ignored. Maskery et al. [27] reported that the pore-size and shape distribution were unaffected by the heat treatment before the melting behavior appears. The dark gray regions in the OM images represent the partial melted QC phase which presents a homogenous distribution before and after heat treatment. Furthermore, the partial melted QC in as-fabricated sample, as shown in Fig. 7 (a), shows a linear arc-like morphology. During the laser melting process, the molten pool illustrates a semi-spherical form and partial melted QC locates at the bottom of molten pool along the boundary due to the higher density of QC. Thus, the partial melted QC possesses a linear arc-liked morphology. The sample, which is heat treated at temperature of 480 °C, shows the similar linear arc-liked partial melted QC (see in Fig. 7 (b)). As the heat treated temperature increases to 540 °C, the partial melted QC changes from linear arc-like some granular (Fig. 7 (c)), due to the low surface energy of granular morphology. In majority, this morphological transformation of the partial melted QC is finish in the case of heat treated at 570 °C (Fig. 7 (d)).

The etched microstructures (Keller solution) with high magnification are presented in Fig. 8. The as-fabricated sample shows an inhomogeneous microstructure consists by Al-rich region, partial melted QC and reacted fine region (as indicated in Fig. 8 (a)). The under reason for this behavior is attributed to the chemical inhomogeneity of powder mixture and ultra-high cooling rate. Even though the powder mixture illustrates a homogenous mixture (Fig. 1 (a)), but the thermal properties of those two powders, such as thermal conductivity, melting temperature etc., are quite different. It leads to complex temperature gradient in molten pool, combined the rapid solidification, and then results the inhomogeneous microstructure. The Al rich region and linear QC are also observed in the sample heat treated at 480 °C (Fig. 8 (b)). As the heat treatment temperature is superior to 540 °C, the Al-rich region was eliminated (see in Fig. 8(c and d)). Moreover, the morphologies of partial melted QC change from linear to granular (Figs. 7 and 8).

According to the XRD pattern (Fig. 3), a novel Al-rich QC phase was *in-situ* formed and then the effect of heat treatment on its microstructure is presented in Fig. 9. As shown in Fig. 9 (a), the as-fabricated sample presents an inhomogeneous microstructure composed by α-Al (Cu) and composite region. The *in-situ* formed QC presents an ultra-fine microstructure, grain size inferior 1 μm with particulate morphology. Furthermore, it can be seen that some *in-situ* QC illustrate pentagon or five-pointed star form. The Kikuchi pattern (see in Fig. 9 (c)) of the *in-situ* QC shows a clearly 5-fold symmetry, which confirms the quasi-crystalline structure. Fig. 9 (b) shows that the *in-situ* QC particle

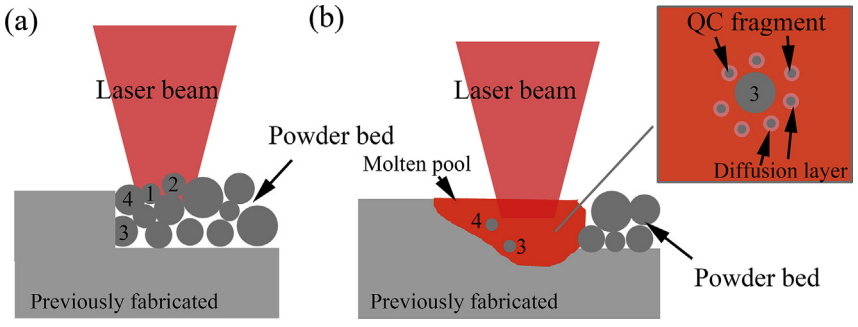

Fig. 5. Schematic illustration of the melting, reacting and solidification behavior of QC reinforcement during SLM process.

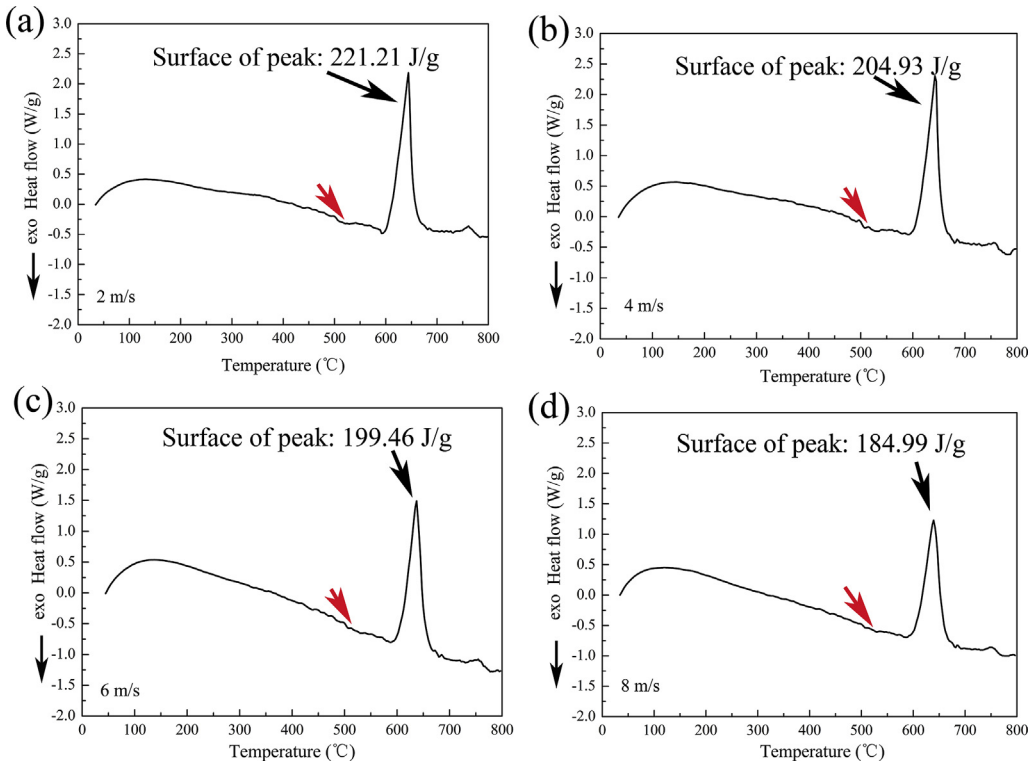

Fig. 6. DSC curves of SLM processed sample at several laser scanning speeds (a) 2 m/s, (b) 4 m/s, (c) 6 m/s and (d) 8 m/s.

changes from dense particulate to porous irregular morphology after heat treatment at 540 °C. It can be attributed to the low cooling rate of heat treatment, similar results was also reported in our previous work in case of different laser scanning speed. The reticulate QC structure can be observed in the heat treated sample. Compared with clearly 5-fold symmetric feature of as-fabricated sample, the Kikuchi pattern of heat treated QC is relative dim with 5-fold (Fig. 9 (d)).

The microhardness of SLM processed samples with several heat treatment temperatures ranged from 25 °C to 570 °C are presented in Fig. 10. As heat treatment temperature rises from room temperature to

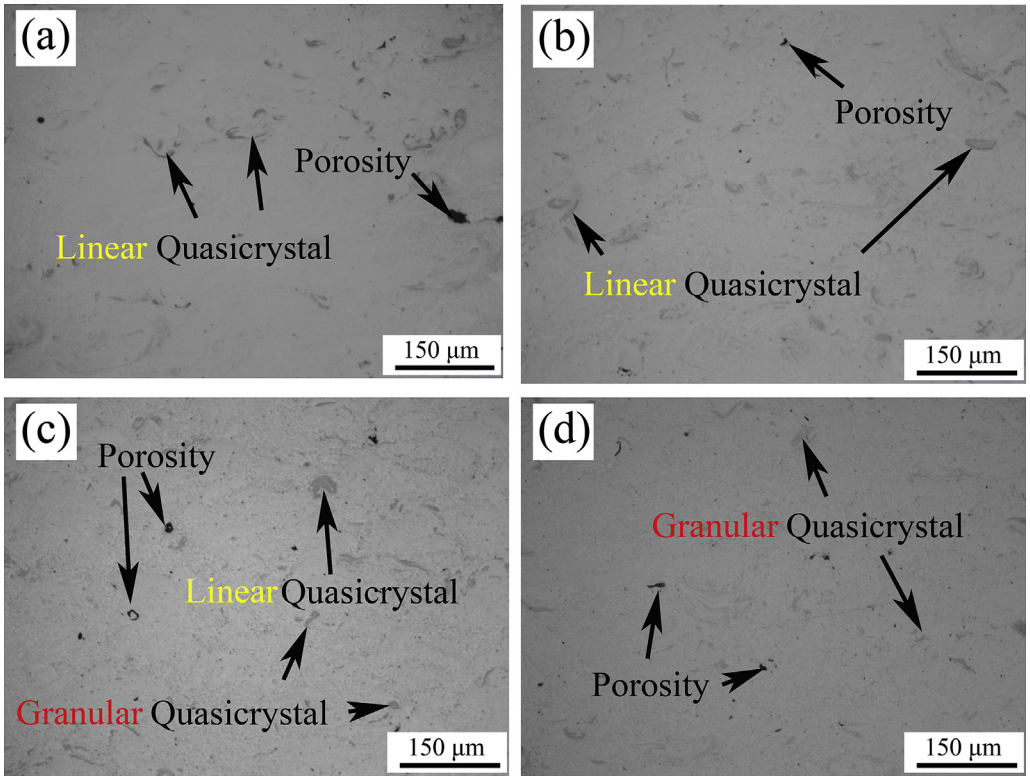

Fig. 7. Low magnification OM images of (a) as-fabricated and normalizing at (b) 480 °C, (c) 540 °C and (d) 570 °C.

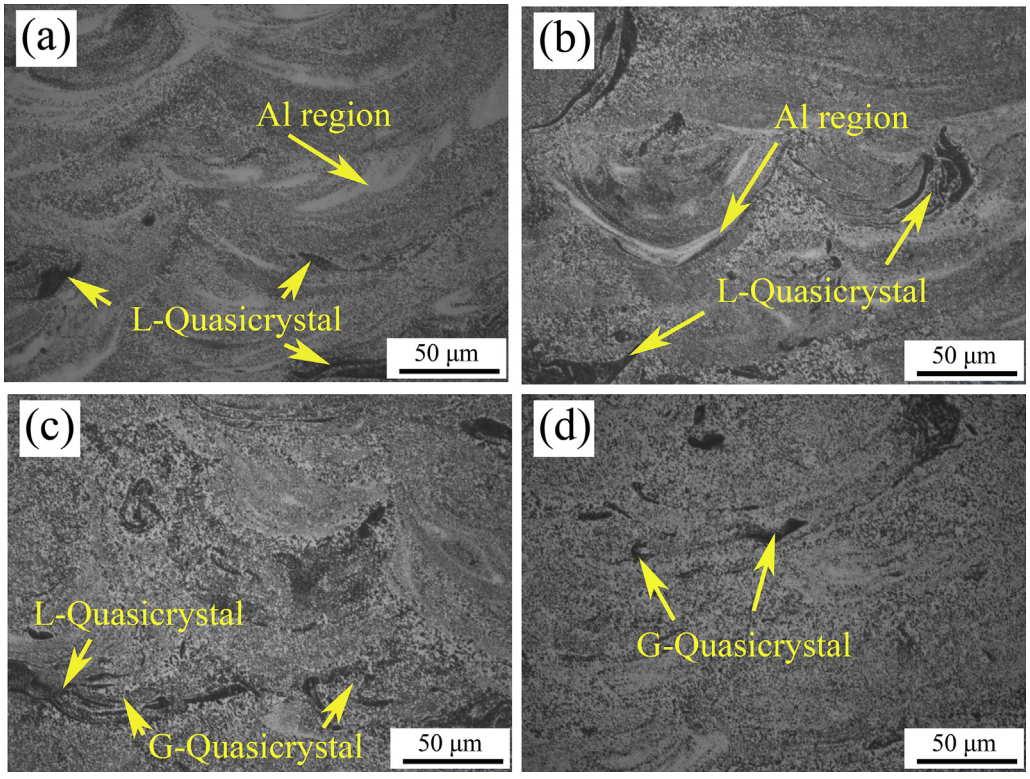

Fig. 8. High magnification OM images (after etching) of (a) as-fabricated and heat treated at (b) 480 °C, (c) 540 °C and (d) 570 °C (L: linear, G: granular).

570 °C, the microhardness fall slightly from 180 HV to 155 HV. For the as-fabricated sample, due to the large atom size of copper, the supersaturated copper causes the lattice distortion and high microhardness. As the heat treatment temperature increases, the copper element precipitates from the supersaturated Al(Cu) solid solution. Therefore, the hardness of SLM processed sample decreases after heat treatment. Additionally, the QC phase grows from irregular dense structure to porous structure after heat treatment, from our previous work [28], which also induces the decrement behavior of microhardness.

The representative stress-strain curves of as-fabricated and heat

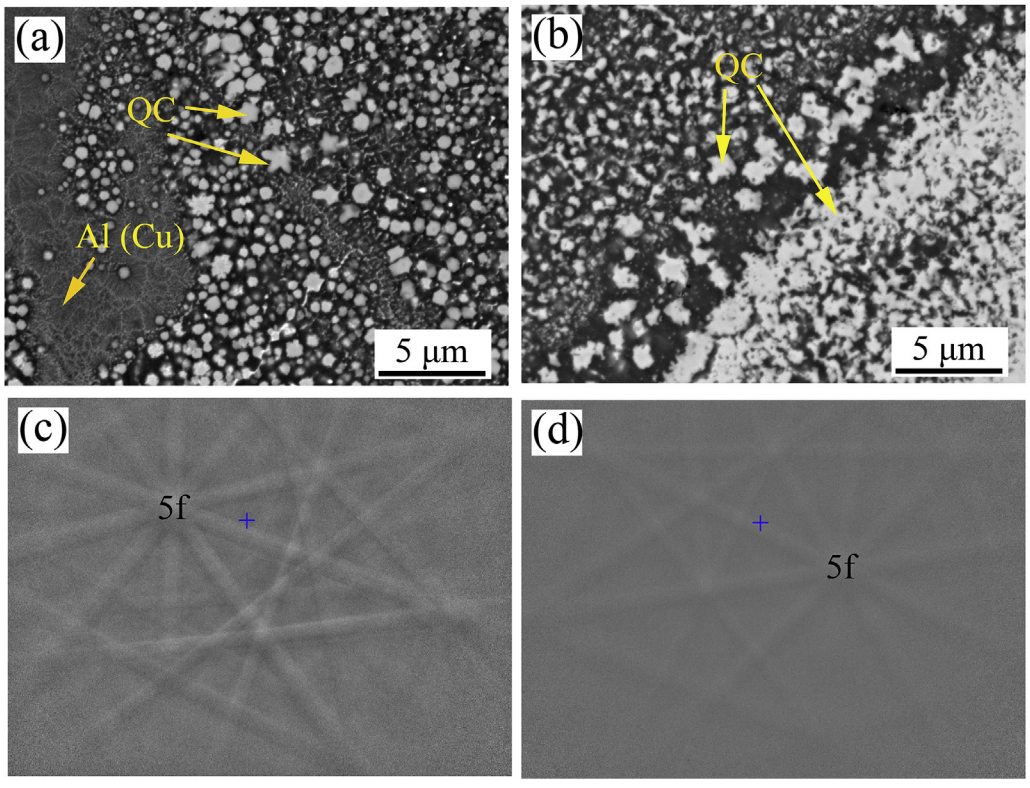

Fig. 9. SEM images of the microstructure and Kikuchi pattern of in-situ formed QC of (a, c) as-fabricated sample and (b, d) heat treated sample at 540 °C.

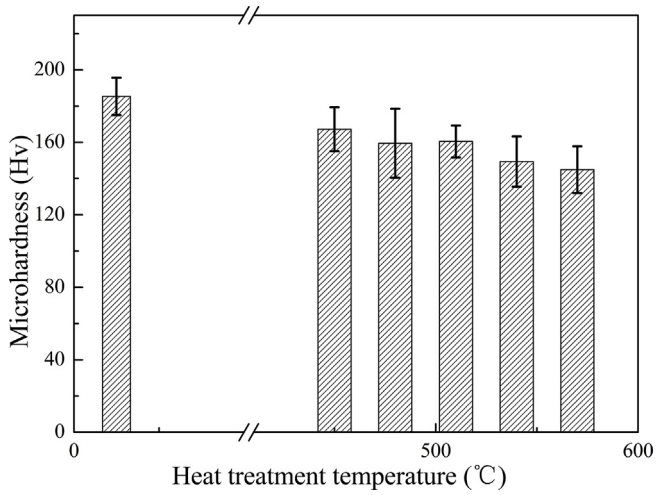

Fig. 10. Microhardness of SLM processed samples with several heat treatment temperatures ranged from 25 °C to 570 °C.

treated at 480 °C, 540 °C and 570 °C samples are shown in Fig. 11. It can be seen that all the four curves present typical three-stages composite tensile results. The tensile procedure could be divided into three steps: (1) high Young modulus at beginning; (2) a stable low Yong modulus stage, (3) the fracture failure. As shown in Fig. 11 (a), the as-fabricated sample possesses ultimate tensile strength (UTS) of 292 MPa, which is similar to well investigated SLMed Al-12Si of 300 MPa [22]. Moreover, our previous work [28] indicated that the wear resistance of this kind of composite is even higher than that of SLM processed hypereutectic Al-Si alloys, which is used as wear resistant device. The UTS remains the similar value for the as-fabricated and heat treated at 480 °C samples (see in Fig. 11 (b)). As the heat treatment temperature increases from 480 °C to 570 °C, the UTS value decreases slight from 291 MPa to 278 MPa (Fig. 11(c and d)). The elongation at failure presents the similar tendency with UTS. However, for stable Young modulus, it increases continually from 3.14 GPa to 3.61 GPa. Unlike the conventional alloy, a reticulate QC structure was formed after heat treatment, which hinders the movement of QC. Thus, the load tends to be applied directly on QC, which possesses high module Young and low ductility. Additionally, tensile toughness (or, deformation energy, UT) is calculated by using area underneath the stress–strain (σ–ε) curve: UT = Area underneath the stress–strain (σ–ε) curve = $\sigma \times \varepsilon$ (U:J·m^{-3}·10^{4}). The tensile toughness decreases from 1352 U to about 1000 U after heat treated at temperature over 490 °C, due to the growth of QC phases and the formation of reticulate QC structure. The slight toughness increment of sample heat treated at 570 °C can be attributed to growth of α-Al grain with high ductility (Fig. 11 (d)).

The fracture surface morphologies of SLM processed samples, in conditions of as-fabricated and heat treated, are presented in Fig. 12 and Fig. 13 at several magnifications. As shown in Fig. 12(a and b), the clear cleavage can be observed in the sample as-fabricated and heat-treated at 480 °C. As mentioned by Suryawanshi et al. [29], this large cleavage surface in correspond to laser traces and interfacial region of

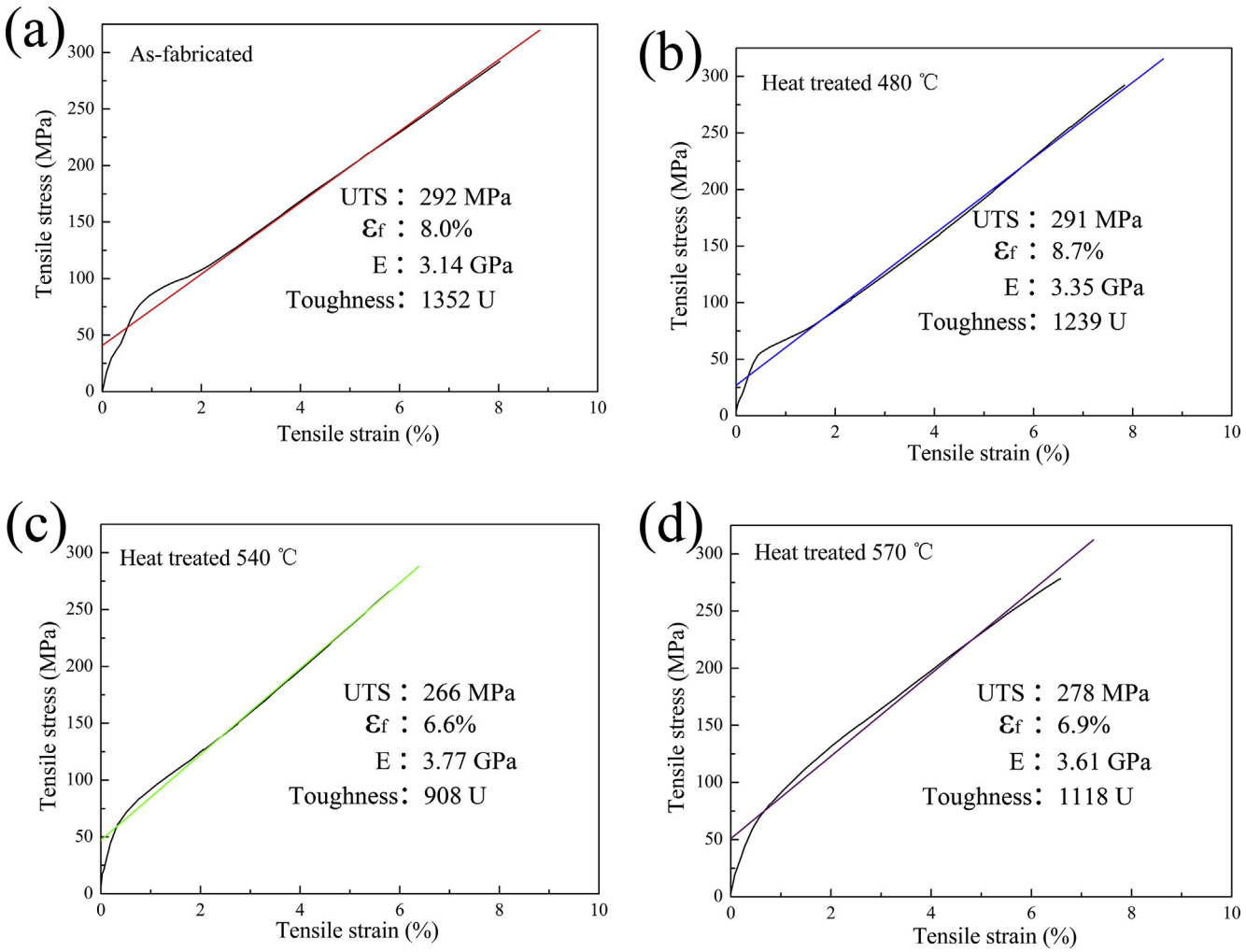

Fig. 11. Tensile curves of (a) as-fabricated and normalizing at (b) 480 °C (c) 540 °C and (c) 570 °C (U: J·m^{-3}·10^{4}).

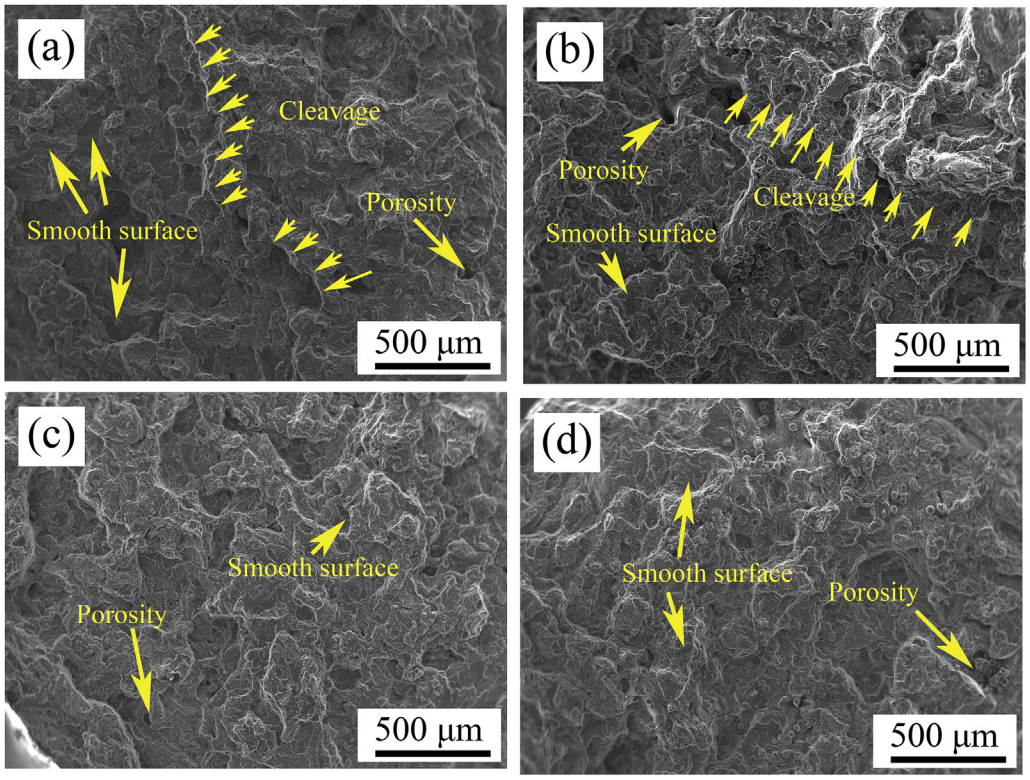

Fig. 12. Low magnification SEM image of fracture surface of (a) as-fabricated and normalizing at (b) 480 °C (c) 540°Cand (c) 570 °C.

molten pool, of which bonding strength is relative weak and easy to fracture. When the heat treatment temperature increases, the interfacial region could be reinforced by the diffusion process. Therefore, the large cleavage surface disappears in the sample heat treated at higher temperature of 540 °C and 570 °C (Fig. 12(c and d)). Additionally, porosity and smooth fracture surface could be also observed in the as-fabricated and heat treated samples.

Fig. 13 shows the fracture surfaces with more details about smooth fracture surface, which corresponds to the fracture of QC particle during tensile test. In the cases of as-fabricated and heat treated at 480 °C (Fig. 13(a and b)), the QC fracture surfaces illustrate large area fraction with the interfaces between QC particle and Al matrix. With the increment of heat treatment temperature, area of QC fractures decreases and disperses into some small fragments (Fig. 13(c and d)). It

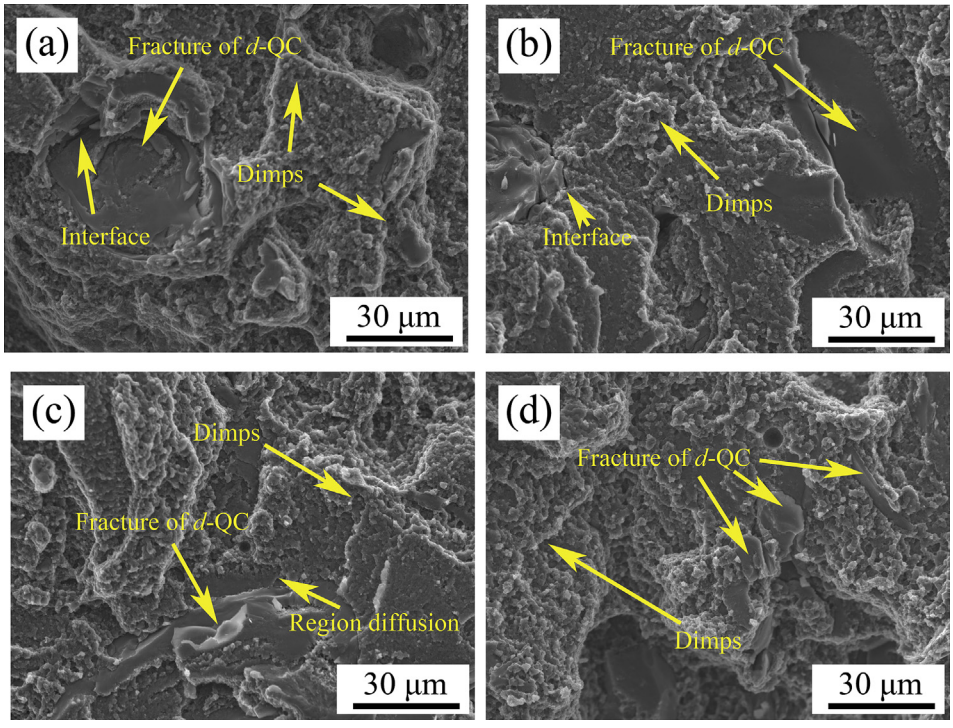

Fig. 13. High magnification SEM image of fracture surface of (a) as-fabricated and normalizing at (b) 480 °C (c) 540°Cand (c) 570 °C.

may be the reason for the decrement of UTS after the heat treatment at high temperature, because of the high tensile strength of QC phases. Moreover, the interface is no longer clear as the result of diffusion region's formation (as shown in Fig. 13 (c)).

4. Conclusion

A novel Al-Fe-Cr quasicrystal reinforced Al matrix composite with high relative density (99%) is prepared by selective laser melting process from the powder mixture.

(1) As the laser scanning speed decreases, the cooling rate of molten pool decreases. A phase transition from d- QC to i- QC appears.
(2) The interfacial analysis, between partial melted QC and Al matrix, indicates that the QC is firstly decomposed into small fragment. And then, the diffusions between QC fragment and Al matrix induce to the phase transition from Al-Cu-Fe-Cr QC to Al-Fe-Cr QC.
(3) The microstructure of as-fabricated sample could be affected and normalized by heat treatment over 500 ˚C as the results of diffusion behavior between QC and matrix-Al.
(4) Moreover, due to the precipitation of copper from supersaturated Al (Cu) solid solution and growth of QC, both the microhardness and tensile strength decreases with the increment of heat treated temperature.

Acknowledgement

The work was supported by the National Key Research and Development Programme of China (Grant No. 2016YFB1100100). The authors are also grateful for the financial support provided by Marie Curie FP7-IPACT-268696(EU) grant.

Appendix A. Supplementary data

Supplementary data related to this article can be found at https://doi.org/10.1016/j.compositesb.2018.08.108.

References

[1] Shechtman D, Blech I, Gratias D, Cahn JW. Metallic phase with long-range orientational order and No translational symmetry. Phys Rev Lett 1984;53:1951–3.
[2] Inoue A. Amorphous, nanoquasicrystalline and nanocrystalline alloys in Al-based systems. Prog Mater Sci 1998;43:365–520.
[3] Dubois JM. The applied physics of quasicrystals. Phys Scripta 1993(T49A), Accessed date: 17 January 2007.
[4] Galano M, Audebert F, Stone IC, Cantor B. Nanoquasicrystalline Al-Fe-Cr-based alloys. Part I: phase transformations. Acta Mater 2009;57:5107–19.
[5] Galano M, Audebert F, Garcia Escorial A, Stone IC, Cantor B. Nanoquasicrystalline Al-Fe-Cr based alloys. Part II: mechanical properties. Acta Mater 2009;57:5120–30.
[6] Fu Y, Kang N, Liao H, Gao Y, Coddet C. An investigation on selective laser melting of Al-Cu-Fe-Cr quasicrystal: from single layer to multilayers. Intermetallics 2017;86:51–8.
[7] Guo X, Chen J, Yu H, Liao H, Coddet C. A study on the microstructure and tribological behavior of cold-sprayed metal matrix composites reinforced by particulate quasicrystal. Surf Coating Technol 2015;268:94–8.
[8] Li RT, Murugan VK, Dong ZL, Khor KA. Comparative study on the corrosion resistance of Al–Cr–Fe alloy containing quasicrystals and pure Al. J Mater Sci Technol 2016;32:1054–8.
[9] Li RT, Dong ZL, Khor KA. Al-Cr-Fe quasicrystals as novel reinforcements in Ti based composites consolidated using high pressure spark plasma sintering. Mater Des 2016;102:255–63.
[10] Wang X, Jiang M, Zhou Z, Gou J, Hui D. 3D printing of polymer matrix composites: a review and prospective. Compos B Eng 2017;110:442–58.
[11] Hu Y, Cong W, Wang X, Li Y, Ning F, Wang H. Laser deposition-additive manufacturing of TiB-Ti composites with novel three-dimensional quasi-continuous network microstructure: effects on strengthening and toughening. Compos B Eng 2018;133:91–100.
[12] Gu DD, Ma C, Xia M, Dai D, Shi Q. A multiscale understanding of the thermodynamic and kinetic mechanisms of laser additive manufacturing. Engineering 2017;3:675–84.
[13] Kang N, Coddet P, Chen C, Wang Y, Liao H, Coddet C. Microstructure and wear behavior of in-situ hypereutectic Al-high Si alloys produced by selective laser melting. Mater Des 2016;99:120–6.
[14] Pauly S, Löber L, Petters R, Stoica M, Scudino S, Kühn U, Eckert J. Processing metallic glasses by selective laser melting. Mater Today 2013;16:37–41.
[15] Kang N, Coddet P, Ammar MR, Liao H, Coddet C. Characterization of the microstructure of a selective laser melting processed Al-50Si alloy: effect of heat treatments. Mater Char 2017;130:243–9.
[16] Thijs L, Kempen K, Kruth JP, Van Humbeeck J. Fine-structured aluminium products with controllable texture by selective laser melting of pre-alloyed AlSi10Mg powder. Acta Mater 2013;61:1809–19.
[17] Suryawanshi J, Prashanth KG, Ramamurty U. Tensile, fracture, and fatigue crack growth properties of a 3D printed maraging steel through selective laser melting. J Alloy Comp 2017;725:355–64.
[18] Yang J, Yu H, Yin J, Gao M, Wang Z, Zeng X. Formation and control of martensite in Ti-6Al-4V alloy produced by selective laser melting. Mater Des 2016;108:308–18.
[19] Han Q, Geng Y, Setchi R, Lacan F, Gu D, Evans SL. Macro and nanoscale wear behaviour of Al-Al2O3 nanocomposites fabricated by selective laser melting. Compos B Eng 2017;127:26–35.
[20] Wang P, Gammer C, Brenne F, Niendorf T, Eckert J, Scudino S. A heat treatable TiB2/Al-3.5Cu-1.5Mg-1Si composite fabricated by selective laser melting: microstructure, heat treatment and mechanical properties. Compos B Eng 2018;147:162–8.
[21] Wang P, Deng L, Prashanth KG, Pauly S, Eckert J, Scudino S. Microstructure and mechanical properties of Al-Cu alloys fabricated by selective laser melting of powder mixtures. J Alloy Comp 2018;735:2263–6.
[22] Kang N, Coddet P, Dembinski L, Liao H, Coddet C. Microstructure and strength analysis of eutectic Al-Si alloy in-situ manufactured using selective laser melting from elemental powder mixture. J Alloy Comp 2017;691:316–22.
[23] Martin JH, Yahata BD, Hundley JM, Mayer JA, Schaedler TA, Pollock TM. 3D printing of high-strength aluminium alloys. Nature 2017;549:365–9.
[24] Dubois JM, Dong C, Janot C, Boissieu MD, Audier M. The reversible crystal-quasicrystal transitions in icosahedral Al-Cu-Fe alloys. Phase Transitions 1991;32:3–28.
[25] Bergmann JP, Petzoldt F, Schürer R, Schneider S. Solid-state welding of aluminum to copper-case studeis. Weld World 2013;57:541–50.
[26] International ASM. ASM metals handbook volume 3 alloy phase diagrams. 1994.
[27] Maskery I, Aboulkhair NT, Corfield MR, Tuck C, Clare AT, Leach RK, Wildman RD, Ashcroft IA, Hague RJM. Quantification and characterization of porosity in selectively laser melted Al–Si10–Mg using X-ray computed tomography. Mater Char 2016;111:193–204.
[28] Kang N, Fu Y, Coddet P, Guelorget B, Liao H, Coddet C. On the microstructure, hardness and wear behavior of Al-Fe-Cr quasicrystal reinforced Al matrix composite prepared by selective laser melting. Mater Des 2017;132:105–11.
[29] Suryawanshi J, Prashanth KG, Scudino S, Eckert J, Prakash O, Ramamurty U. Simultaneous enhancements of strength and toughness in an Al-12Si alloy synthesized using selective laser melting. Acta Mater 2016;115:285–94.